Search for Ultra High Energy Neutrinos with AMANDA

Andrea Silvestri* for the IceCube Collaboration†

**Department of Physics and Astronomy, University of California, Irvine, CA 92697, USA.*
†*See the special section of these proceedings.*

***Abstract*. We present results from the search for diffusely distributed Ultra High Energy (UHE) neutrinos performed on data collected in 2003-2005 with the AMANDA experiment. At energies above a few PeV the Earth is opaque to neutrinos, therefore neutrinos must be differentiated from downward going cosmic ray induced (bundles of) muons. A search for a diffuse flux of UHE neutrinos shows no events, leading to a flux limit, summed over all flavors $\mathbf{E^2\Phi_\nu \leq 8.4 \times 10^{-8}}$ GeV cm^{-2} s^{-1} sr^{-1} (90% confidence level) for $\mathbf{10^{15.2}}$ eV $< \mathbf{E_\nu} < \mathbf{10^{18.8}}$ eV. This limit is the most stringent placed to date. A number of model predictions different from the $\mathbf{E^{-2}}$ spectrum have been tested and some have been rejected at a 90% C.L. We show that these results can also place a limit on the flux from point sources in the Southern Sky as a function of declination and valid in the same energy range.**

***Keywords*: Diffuse sources, high energy neutrinos, AMANDA**

I. Introduction

Neutrino production from Active Galactic Nuclei (AGN), and other astrophysical sources have been extensively modeled during the past two decades, as described in [1], [2], [3]. Super-massive black holes hosted in the AGNs would accelerate, via a first-order Fermi mechanism, charged particles to ultra high energies. The collision of ultra-relativistic protons with the photon field in the AGN, via pγ and pp-interactions, would then produce high-energy neutrinos. The predicted intensity of neutrinos from these astronomical sources can reach the Earth and be detected by underground neutrino telescopes. Other theoretical calculations as presented in [4], [5], [6] and [2], derive an upper bound to the expected neutrino fluxes from high energy cosmic ray observations. These predictions, based on a model-independent approach, provide also a target for neutrino detector sensitivities. The predicted upper bound (ν_μ and $\bar{\nu_\mu}$ combined) for an E^{-2} spectrum is $E^2\Phi_\nu^{WB} \leq 2 \times 10^{-8}\xi_z$ GeV cm^{-2} s^{-1} sr^{-1}, where ξ_z accounts for cosmological model and source evolution. Using cosmological dependence and source evolution that follows star formation rate over cosmological time gives $\xi_z \sim 3$. Assuming $\nu_\mu/\nu_e = 0.5$ at the source, produced from pγ and pp-collisions, the upper bound on the total flux for all $\nu-$ flavors becomes $E^2\Phi_\nu^{WB} \sim 9 \times 10^{-8}$ GeV cm^{-2} s^{-1} sr^{-1}.

II. Analysis

The analysis results presented in this paper incorporate 3-year of AMANDA data collected in 2003-2005 (detector live-time of 507 days) and are based on work for one year analysis [7] of 2003 data. The Antarctic Muon And Neutrino Detector Array (AMANDA) [8], is the first neutrino telescope constructed in transparent ice, and deployed between 1500 m and 2000 m beneath the surface of the ice at the geographic South Pole in Antarctica. The AMANDA detector uses the Earth to filter out muons generated in the atmosphere on the Northern hemisphere and to search for point and diffuse sources of neutrinos with upward going direction at TeV to 100 TeV energies. However, at energies above PeV the Earth is opaque to neutrinos, therefore ν's must be differentiated from the large background (billions of events per year) of downward going cosmic ray induced (bundles of) muons, which constitutes the primary challenge of this analysis. AMANDA has been taking data with the same detector configuration since 2000, and the data acquisition electronics was upgraded in 2003 by recording full waveforms of the photo-electron (p.e.) pulses from the photomultiplier tubes (PMT) using Transient Waveform Recorders (TWR) [9]. The entire 2003 data set of the AMANDA TWR technology was processed, calibrated and analyzed to perform an atmospheric neutrino analysis and a search for point sources in the Northern hemisphere sensitive at TeV energies [10], [11], which demonstrated the basic capabilities of the novel system to reproduce comparable physics results of the standard system of the AMANDA detector. After demonstrating the physics performance of the TWR technology, the analysis is performed to search for diffusely distributed neutrinos above PeV energies. The full waveforms from the PMT's provide far more information on the light distribution from complex high energy events. However, the new technology produced $\sim$ 85 TB in 3 years, more than an order of magnitude increase w.r.t. the standard AMANDA system. To meet the challenge of large data structure and to simulate comparable data volume new analysis strategies were developed using high performance computing resources. The resources required for this analysis exceeded 2M CPU hours.

The UHE analysis is performed by using the information of multiple p.e.'s from the PMT waveforms. The initial level of the analysis is defined by eliminating over 90% of the background by retaining only events

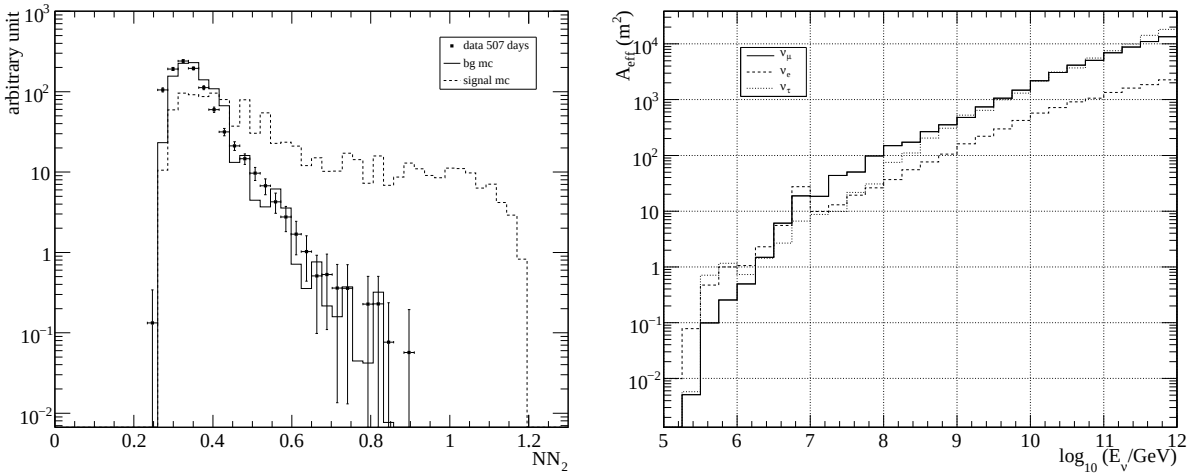

Fig. 1. Left panel: the neural network (NN_2) distribution plotted for data, background and signal simulation. Right panel: detector effective area for muon, electron and tau neutrinos as a function of neutrino energy.

with large number of p.e. pulses recorded in the array. After this level the analysis is refined by developing two independent neural networks. The first neural network mostly incorporates variables from reconstructed events, i.e. the reconstructed zenith angle of the events, which can separate downward going muons from signal mostly concentrated at the horizon. The second neural network uses primarily time dependent variables, like spread in leading edge of the arrival time and time-over-threshold values of the p.e. pulses, which at the higher level of the analysis better discern signal from high energy bundles of atmospheric muons. Variables were developed that exploit the full PMT waveforms, which in turn strongly correlate to signal features and better separate signal-like background events. Selection criteria based on single variable discriminators, like the number of photon-electrons were tested, but demonstrated not to be efficient for retaining signal events. Therefore a new set of variables were developed, which depend on timing and energy of typical signal events [7]. The new developed variables which use multiple photon-electrons in the PMT waveforms are the fluctuation of the time-over-threshold incorporated in the standard deviation of the tot's (σ_{tot}), the mean of the leading edge times of the photon-electron pulses (μ_{le}), and the fluctuation from the standard deviation of the leading edge times (σ_{le}). Simulation of signal shows that distant UHE ν events may not deposit much light in the detector, but the spread in leading edge arrival time σ_{le} and time-over-threshold σ_{tot} values is large compared to typical background events. Background events tend to have large number of muons with relatively small lateral dimensions, which traverse through or close to the detector. Consequently, the arrival time of background photons shows little spread in time. On the other hand, signal events with comparable values of number of photon-electrons do not pass close to the detector. Therefore, these events differ from background because the photons show large variability in the arrival times. To further improve background rejection, neural networks were developed and trained. The most powerful neural network included variables that measure the mean spread in leading edge times and fluctuations of time-over-threshold values. The search is performed with a blind analysis, i.e. 20% of the data sample is used to compare data with simulation while cut optimization is based on simulation solely. Once the analysis criteria are established, the cuts are frozen and applied to the remaining 80% of the data. Fig. 1 left panel shows the neural network (NN_2) before the final cut level for the combined data set, for the simulated atmospheric background and for the neutrino signal following an E^{-2} spectrum.

Background simulation was performed by generating primary cosmic ray using the CORSIKA package [12], propagating particles through the ice with the program MMC [13], recording detector response using the program AMASIM [14] with description of depth-dependent properties of Antarctic ice [15], and including proper treatment of waveform data. Similarly, neutrino signal simulation was performed for all flavors using the program ANIS [16]. Background simulation was biased in energy and spectrum towards high energy events to accommodate available computing resources. The final cut on NN_2 was determined by evaluating the model rejection factor (MRF), as described in [17], and computing the minimum of the ratio $\mathrm{MRF} = \langle \mu_{90}(n|b) \rangle / n_{sig}$. The $\langle \mu_{90}(n|b) \rangle$ is the average 90% C.L. upper limit, determined by using the Feldman-Cousins method [18], computed over the Poisson probabilities for the experiment repeated many times, and n_{sig} is the number of signal events for a given model. The minimum of the MRF determines the cut which is set to $NN_2 > 0.85$. After the final cut one experimental event is observed over a detector live-time of 507 days, consistent with 0.9 $(-0.9, +1.3)$ events from background expectation.

III. RESULTS

The search for a diffusely distributed flux of UHE neutrinos shows no signal events, leading to a prelimi-

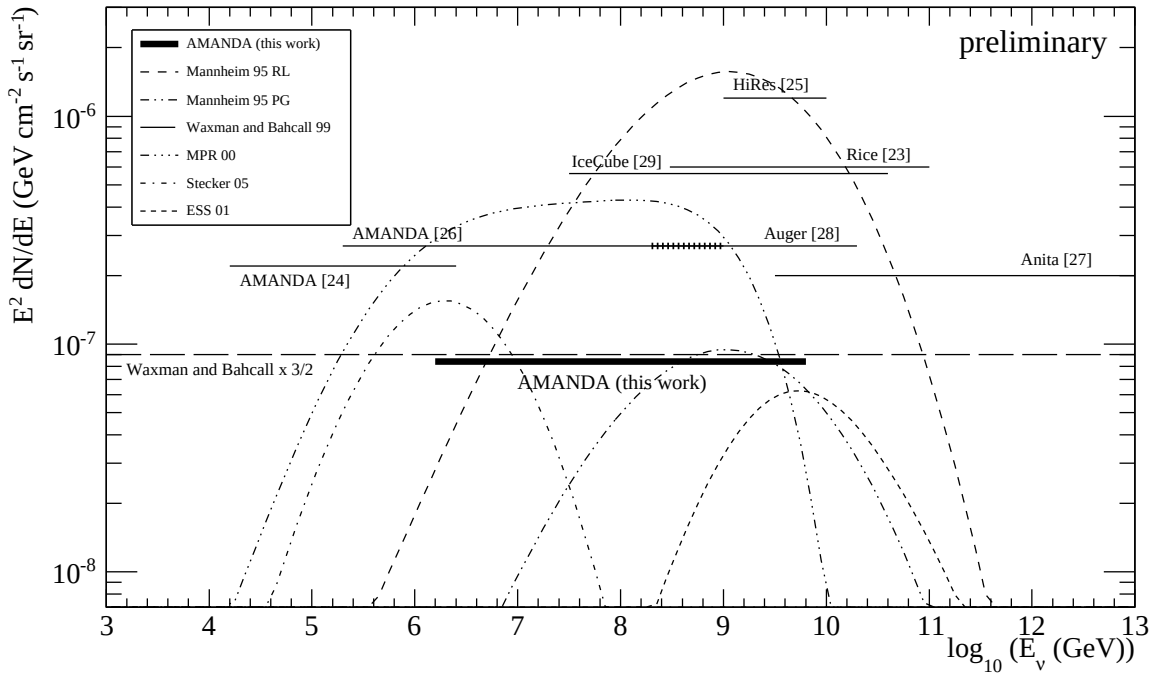

Fig. 2. Experimental limits of this analysis on a diffuse E^{-2} ν-flux for all flavors as a function of neutrino energy, thick solid line. Solid lines represent experimental limits from other experiments [23], [24], [25], [26], [27], [28], [29]. Dotted curves represent model predictions for a diffuse ν-flux, and predictions have been adjusted for all flavor neutrino contribution, where necessary.

nary flux limit, summed over all flavors

$$E^2\Phi_\nu \leq 8.4 \times 10^{-8}\ \mathrm{GeV\ cm^{-2}\ s^{-1}\ sr^{-1}} \quad (1)$$

at 90% C.L. for the energy interval $10^{15.2}$ eV $< E_\nu <$ $10^{18.8}$ eV, defined by the 90% containment of the final neutrino energy distribution, which has a median energy of $\langle E_\nu \rangle = 4 \times 10^{16}$ eV. Fig. 1 right panel shows the detector effective area for all flavor neutrinos for an E^{-2} spectrum as a function of neutrino energy, which for muon neutrinos reaches 100 m^2 for 100 PeV and rapidly increases with energy.

The limits are computed including the contribution of systematic uncertainties by using the method described in [19]. Tab. I summarizes the different sources of systematic uncertainties which impact background and signal simulation in this analysis: The same numbers as given in the table is then repeated in the text. Differences in the simulation for cosmic ray composition by generating proton and iron CR primaries, and interaction models by using two different hadronic models (QGSJET and SIBYLL) were used to estimate variations in background event rate; Uncertainties in detector sensitivity which mostly depend on the absolute sensitivity of the PMT's, were also included; Variations have been estimated due to the difference in detector response observed for the three years studied in the analysis; Variations in the spread of the time-over-threshold for distances $d > 200$ m were evaluated for the impact on signal efficiency; Studying ice properties with two different models gave a max variation of 16% in signal sensitivity; The impact on systematic uncertainties due to ice properties has been further studied by varying the length of photon propagation in ice for distances characteristic of high energy signal, and by incorporating this variation into the effect of detector sensitivity to estimate the impact on signal sensitivity; Background from charm production has been estimated to be negligible in this analysis;

TABLE I
SUMMARY OF SYSTEMATIC UNCERTAINTIES ESTIMATED FROM DIFFERENT SOURCES IMPACTING BACKGROUND AND SIGNAL SIMULATION.

Source	bg	signal (E^{-2})
CR comp. and inter. models	$\pm 80\%$	-
detector sensitivity	$\pm 15\%$	$\pm 15\%$
year-to-year detector variation	$\pm 14\%$	$\pm 14\%$
tot-factor for $d > 200$ m	-	$+10\%$
ice properties	$\pm 20\%$	$\pm 20\%$
charm BG	negl.	-
tot-corr. and N_2-laser cal.	$\pm 100\%$	$\pm 10\%$
neutrino cross section [20]	-	$\pm 4\%$
LPM effect	-	-3%
total (added in quadrature)	$\pm 131\%$	$\pm 32\%$

TABLE II
SUMMARY OF MODEL PREDICTIONS TESTED BY THIS ANALYSIS. MODELS WITH A MRF < 1 ARE EXCLUDED AT 90%, WHILE MODELS WITH A MRF > 1 ARE CONSISTENT WITH THESE RESULTS.

Model	ν_{all}	MRF	Reference
AGN RL A-*jet*	1.10	3.05	Mannheim 95 PG [1]
AGN RL B-*jet*	17.8	0.19	Mannheim 95 RL [1]
AGN-*jet*	14.6	0.23	MPR 00 [2]
AGN-*core*	3.12	1.07	Stecker 05 [3]
Waxman-Bahcall	4.04	0.83	WB 99 [4]
GZK mono-energetic	5.50	0.61	KKSS 02 [21]
GZK index α=2	4.68	0.72	KKSS 02 [21]
GZK full evol.	0.28	12.0	ESS 01 [22]

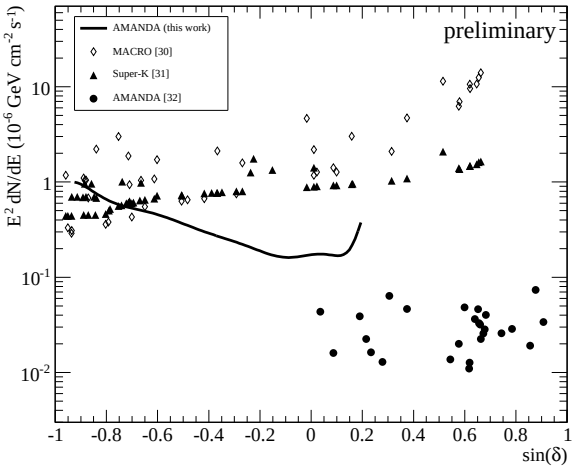

Fig. 3. Point flux limits as a function of declination $sin(\delta)$ for the Southern Sky averaged over azimuth, solid line. Also included are limits from other experiments [30], [31] and for the Northern Sky [32].

Variations in the N_2-laser calibration for the spread of the time-over-threshold were estimated for background event rate and signal efficiency; Uncertainties in the neutrino cross section [20] for energies relevant for this analysis were incorporated, and impact due to LPM effect for signal above 10^8 GeV were also included. The estimated systematic uncertainties have been added in quadrature and incorporated in the final results of the analysis.

The diffuse limit has been used to test a number of model predictions different from the E^{-2} spectrum. Model predictions with a ratio $\langle \mu_{90}(n|b) \rangle / n_{sig} < 1$ are excluded by this analysis. The models tested and the corresponding MRF have been summarized in Tab. II. A class of AGN predictions based on *jet-models* scenario, such as [1] (RL B) and [2] have been excluded, while prediction [1] (RL A) is not, and AGN prediction based on *core-models* scenario [3] is almost excluded. From the class of models excluded by this analysis we can conclude *jet-models* normalized to diffuse x-ray or GeV/TeV emission from individual sources are generally disfavored. These limits are consistent, and below the maximum upper bound to neutrino flux predicted by [4], [6], and also below the maximum neutrino flux due to possible extra-galactic component of low-energy protons of 10^{17} eV [5]. These results are also consistent and below the bounds on neutrino fluxes presented by [2], computed by assuming optically thin (thick) sources to pion photo-production processes. Models on GZK neutrino spectrum were also tested, predictions [21] are excluded, while prediction [22] is still compatible with these results. The limits from this work to an E^{-2} neutrino flux as a function of energy are shown in Fig. 2, thick solid line. Model predictions are represented by dotted curves, and solid lines show limits presented by other experiments [23], [24], [25], [26], [27], [28], [29].

At UHE energies this analysis is sensitive to search for point source of neutrinos in the Southern Sky. Simulation shows that muons are reconstructed with angular resolution of $\sim 7^o$ over the entire Southern hemisphere. Except for a small band near the horizon, signal originating from the Southern Sky will be observed in the Southern Sky. The sensitivity only depends on zenith angle and is roughly independent of azimuth, and maximum sensitivity peaks at the horizon [7]. Since, no excess of events were observed, a flux limit as a function of declination is derived, Fig. 3, and fitted with a function of δ, as $E^2 dN/dE_\nu(\sin\delta) \leq [1.3 \times e^{-(2\ sin\ \delta)}] \times 10^{-7}$ GeV cm^{-2} s^{-1} with 10% accuracy, valid for $-0.98 < sin(\delta) < 0$, and for $10^{15.2}$ eV $< E_\nu < 10^{18.8}$ eV. These point flux limits are valid for energies above PeV, and are compatible with results from other experiments, which cover lower energy intervals between 10 GeV - 100 TeV [30], and between 10 GeV - 100 GeV [31].

To summarize, we have presented in this paper the most stringent limits to date for neutrino energies above 1 PeV. These experimental limits begin to restrict the largest possible fluxes of the WB upper bound [4], [5], [6].

IV. Acknowledgment

The author acknowledges support from U.S. National Science Foundation-Physics Division, and the NSF-supported TeraGrid system at the San Diego Supercomputer Center (SDSC).

References

[1] K. Mannheim, *Astropart. Phys.* **3**, 295 (1995).
[2] K. Mannheim et al., *Phys. Rev. D* **63**, 023003 (2001).
[3] F. Stecker, *Phys. Rev. D* **72**, 107301 (2005).
[4] E. Waxman and J. Bahcall, *Phys. Rev. D* **59**, 023002 (1999).
[5] J. Bahcall and E. Waxman, *Phys. Rev. D* **64**, 023002 (2002).
[6] E. Waxman, *Phil.Trans.Roy.Soc.Lond.* **A 365**, 1323 (2007).
[7] A. Silvestri, *Ph.D. Thesis*, University of California, Irvine (2008).
[8] E. Andres et al., *Nature* **410**, 441 (2001).
[9] W. Wagner et al., *Proc. 28th ICRC*, **2**, 1365 (2003).
[10] A. Silvestri et al., *Proc. 29th ICRC*, **5**, 431 (2005).
[11] A. Silvestri et al., *Mod. Phys. Lett. A* **22**, 1769 (2007).
[12] D. Heck, *DESY-PROC-1999-01*, 227 (1999).
[13] D. Chirkin and W. Rhode, *hep-ph/0407075* (2004).
[14] S. Hundertmark,*Proc.1st νTelescopes Workshop*, Zeuthen (1998).
[15] M. Ackermann et al., *J. Geophys. Res.* **111**, D13203 (2006)
[16] M. Kowalski and A. Gazizov, *Comput. Phys. Comm.* **172**, 203 (2005).
[17] G. Hill and K. Rawlins, *Astropart. Phys.* **19**, 393 (2003).
[18] G. J. Feldman and R. D. Cousins, *Phys. Rev. D* **57**, 3873 (1998).
[19] G. Hill, *Phys. Rev. D* **67**, 118101 (2003).
[20] A. Cooper-Sarkar and S. Sarkar, *JHEP* **75**, 801 (2008).
[21] O. E. Kalashev et al., *Phys. Rev. D* **66**, 063004 (2002).
[22] R. Engel et al., *Phys. Rev. D* **64**, 093010 (2001).
[23] I. Kravchenko et al., *Phys. Rev. D* **73**, 082002 (2006).
[24] A. Achterberg et al., *Phys. Rev. D* **76**, 042008 (2007).
[25] K. Martens et al., *astro-ph/0707.4417*, (2007).
[26] M. Ackermann et al., *Astrophys. J.* **675**, 1014 (2008).
[27] P. Gorham et al., *astro-ph/0812.2715*, (2008).
[28] J. Abraham et al., *astro-ph/0903.3385*, (2009).
[29] K. Mase, A. Ishihara and S. Yoshida et al., *Proc. 31th ICRC*, these Proceedings (2009).
[30] M. Ambrosio et al., *Astrophys. J.* **546**, 1038 (2001).
[31] S. Desai et al., *Astropart. Phys.* **29**, 42 (2008).
[32] R. Abbasi et al., *Phys. Rev. D* **79**, 062001 (2009).